scientific reports



OPEN

Extremely low-frequency electromagnetic fields facilitate proliferation and functional differentiation in spinal neural stem cells

Wenxu Tang^{1,2}, Dan He³, Xiaofei Li^{1,2,4}, Yi Feng⁵, Yue Xu^{1,2}, Jiawei Hu^{1,2}, Wei Xu^{6,7 \boxtimes} & Lei Xue^{1,2,4 \boxtimes}

Traumatic spinal cord injury (SCI), typically resulting from direct mechanical damage to the spine, often leads to disruption of neural signaling and axonal conduction, severely impairing nervous system function. In rodent models of SCI, neural stem cell (NSC) transplantation has demonstrated significant potential in restoring motor function and enhancing neural repair. Additionally, extremely low-frequency electromagnetic fields (ELF-EMFs) have demonstrated efficacy in promoting nerve regeneration and activating spinal circuits. However, studies exploring how ELF-EMFs influence NSC activation remain limited. In this study, using spinal cord-derived NSCs from adult mice, we report that ELF-EMFs enhance cell proliferation and self-renewal by upregulating Sox2 expression. Furthermore, we addressed the underlying mechanisms and found that ELF-EMFs activate T-type calcium channels and enhance calcium currents. The resulting increase in intercellular calcium concentration upregulates the expression of NeuroG1 and NeuroD1, promoting neuronal differentiation of NSCs and enhancing neurite outgrowth. Our findings provide new insights into the ELF-EMF-mediated activation of NSCs and highlight their potential for integration into combination therapies and SCI repair.

Keywords Extremely low-frequency electromagnetic fields, Spinal cord injury, Spinal cord-derived neural stem cells, Cell proliferation, Cell differentiation, Pro-neuronal gene

Spinal cord injury (SCI) is a devastating neurological disorder that affects approximately 1.3 million people worldwide, with around 180,000 new cases occurring annually¹. SCIs typically result from direct mechanical trauma to the spine, which often triggers secondary immunological responses, leading to neurodegeneration and cytotoxicity^{2,3}. These events disrupt axonal transmission in the nervous system, thereby further compromising neurological function⁴. Therefore, the key to SCI repair lies in nerve regeneration and neural circuit reconstruction^{5,6}. However, clinical treatments using neurotrophic factors have limited effects on promoting nerve cell regeneration, while neural stem cell (NSCs) transplantation is an effective method^{6,7}. Recently, breakthroughs in NSCs research have provided a strong theoretical basis for SCI repair^{8,9}.

NSCs are multipotent, self-renewing progenitor cells capable of differentiating into specific neurons or glial cells to help restore disrupted neuronal networks¹⁰. The delicate balance between NSC proliferation and differentiation is tightly regulated by various factors. For example, *Sox2* plays a critical role in maintaining the progenitor state of NSCs¹¹, while the basic Helix-Loop-Helix (bHLH) transcription factor family predominantly

¹Department of Physiology and Neurobiology, School of Life Sciences, Fudan University, Shanghai 200438, China. ²State Key Laboratory of Medical Neurobiology and MOE Frontiers Center for Brain Science, Fudan University, Shanghai 200433, China. ³Institute for Regenerative Medicine, State Key Laboratory of Cardiology and Medical Innovation Center, Frontier Science Center for Stem Cell Research, School of Life Sciences and Technology, Shanghai East Hospital, Tongji University, Shanghai 200092, China. ⁴Research Institute of Intelligent Complex Systems, Fudan University, Shanghai 200433, China. ⁵Department of Critical Care Medicine, Shanghai General Hospital, Shanghai Jiaotong University School of Medicine, Shanghai 200080, China. ⁶Division of Spine, Department of Orthopaedics, Tongji Hospital, Tongji University School of Medicine, Shanghai 200065, China. ⁷Key Laboratory of Spine and Spinal Cord Inury Repair and Regeneration, Tongi University, Ministry of Education, Shanghai 200065, China. [™]email: david_xuwei@tongji.edu.cn; lxue@fudan.edu.cn

governs the differentiation of NSCs¹². Previous studies have shown that transplanted NSCs can aid functional recovery in rodent SCI models^{13,14}. Although NSC transplantation has been demonstrated to be clinically safe, the extent of functional recovery and the underlying mechanisms remain insufficiently documented.

Adult endogenous stem cells (AESCs), located in adult neural tissues, have shown potential for regeneration following SCI in mouse and rat models¹⁵. Additionally, Weiss et al. discovered that epidermal growth factor (EGF) and basic fibroblast growth factor (bFGF) induce the proliferation of spinal neural precursor cells (NPCs)¹⁶, confirming the existence of spinal cord-derived NSCs in spinal cord tissue. Although previous studies have revealed that AESCs primarily proliferate into new glial cells in the spinal cord following acute injury^{15,17,18}, the potential for AESCs, especially spinal cord-derived NSCs, to differentiate into neurons, as well as the underlying molecular mechanisms governing this process, remains unclear.

Extremely low-frequency electromagnetic fields (ELF-EMFs), primarily generated by various household appliances, are alternating electromagnetic fields with frequencies below 300 Hz¹⁹. During the past few decades, considerable evidence has shown that non-thermal exposure to ELF-EMFs can induce biological changes both in vivo and in vitro^{20,21}, including gene expression²², tissue repair²³, and cell proliferation²⁴, all of which are potentially beneficial for treating neurological disorders. Despite accumulating experimental evidence suggesting significant biological effects, the underlying mechanisms remain poorly understood. Previous studies have highlighted the impact of ELF-EMFs at the cellular level²⁵, particularly on the physiological properties of cell membrane and channels^{26–28}. Consequently, neurons are likely to be among the most sensitive cells, as exposure to ELF-EMFs may either excite or suppress neuronal activity through interactions with voltage-gated channels²⁷. Calcium influx through voltage-gated calcium channels (VGCCs) has been shown to trigger signaling pathways that regulate gene expression involved in cell proliferation, apoptosis, and neuronal differentiation²⁹. However, the expression and functional role of VGCCs in spinal cord-derived NSCs during ELF-EMF exposure remain poorly understood.

In this study, we provided direct evidence that ELF-EMFs enhance proliferation and self-renewal of spinal cord-derived NSCs by upregulating *Sox2*. Additionally, ELF-EMFs promote cell differentiation into neurons by activating T-type calcium channels and thereby upregulating pre-neuronal genes, such as *NeuroG1* and *NeuroD1*, which are part of the bHLH transcription factor family. Our findings offer new insights into ELF-EMF-activated functions of NSCs and highlight the potential of combinatorial treatments for clinical applications.

Materials and methods Mice maintenance

C57BL/6 mice were purchased from Shanghai Sippe-Bk Lab Animal Co., Ltd (Shanghai, China) and housed in a Specific Pathogen Free (SPF) animal facility at Fudan University, operating under Biosafety Level 1 (BSL-1) conditions. Mice were housed in groups of five with a 12-h light/dark cycle, ambient temperature of 22 ± 2 °C, and humidity levels maintained at 40–50%. Food and water were provided ad libitum. All animal experiments in this study were conducted in accordance with the guidelines of the Animal Care and Use Committee of Fudan University and ARRIVE guidelines³⁰, with protocols approved by the Institutional Animal Care and Use Committee of Shanghai, China. Mice used in these studies were euthanized by intraperitoneal injection of pentobarbital (100 mg/kg, 100 mg/ml in normal Saline) using a 27 G needle, confirmed by absence of breathing and heartbeat.

Isolation and culture of spinal cord-derived NSCs

NSCs were isolated from the thoracolumbar spinal cords (T1-L5) of 8-week-old adult C57BL/6 mice using a rigorously optimized protocol³¹. Following dorsal skin incision and exposure of the vertebral column, the spine was transected caudally and longitudinally incised along the bilateral margins to expose the spinal cord, which was then gently extracted using forceps. To remove erythrocyte contamination, the harvested tissue was treated with red blood cell lysis buffer (Invitrogen, USA). The spinal cords were minced and enzymatically dissociated in 0.25% trypsin-EDTA (Gibco, USA) supplemented with 20 U/ml DNase I (Thermo Scientific, USA) at 37 °C for 10 min. Digestion was terminated with neurobasal medium (Thermo Scientific, USA) containing 10% fetal bovine serum (FBS, Gibco, USA), and the resulting suspension was filtered through a 40-µm cell strainer (Corning, USA) to remove debris. Cells were centrifuged, resuspended, and cultured in proliferation medium. Cells obtained before the first passage (P0) were defined as primary spinal cord-derived NSCs.

NSCs were cultured in proliferation medium, comprising of a 1:1 (v/v) mixture of Dulbecco's modified Eagle's medium (DMEM) and F12 medium (Gibco, USA), supplemented with B27 (Gibco, USA), N2 (Gibco, USA), bFGF (20 ng/ml; PeproTech, USA), and EGF (10 ng/ml; PeproTech, USA). The cultures were maintained under floating conditions in 25 cm² flask with 5 ml of proliferation medium³¹. Half of the medium was replaced every 3 days. After 7–10 days in vitro, neurospheres were harvested by centrifugation, dissociated using Accutase (Gibco, USA), and collected by centrifugation at 1,000 rpm for 5 min. Cells were resuspended in proliferation medium, and passages two to four (P2-P4) were used for subsequent experiments.

Prior to differentiation, passaged neurospheres were cultured for 1-2 days to allow formation of compact spheres (100–150 μ m diameter). To induce differentiation, the NSCs were cultured on poly-D-lysine (PDL)-coated 35 mm dishes in differentiation medium, where bFGF and EGF were replaced with 1% FBS compared to proliferation medium.

ELF-EMF exposure

The system used for exposing cells to electromagnetic fields was as previously described³². Briefly, spinal cord-derived NSCs were exposed to a 50 Hz magnetic field generated by a pair of Helmholtz coils positioned in opposition. The coils were powered by an AC power generator, producing a sinusoidal input voltage, with magnetic flux densities adjustable between 0.1 and 1.0 mT (Fig. 1A). Throughout the exposure period, the

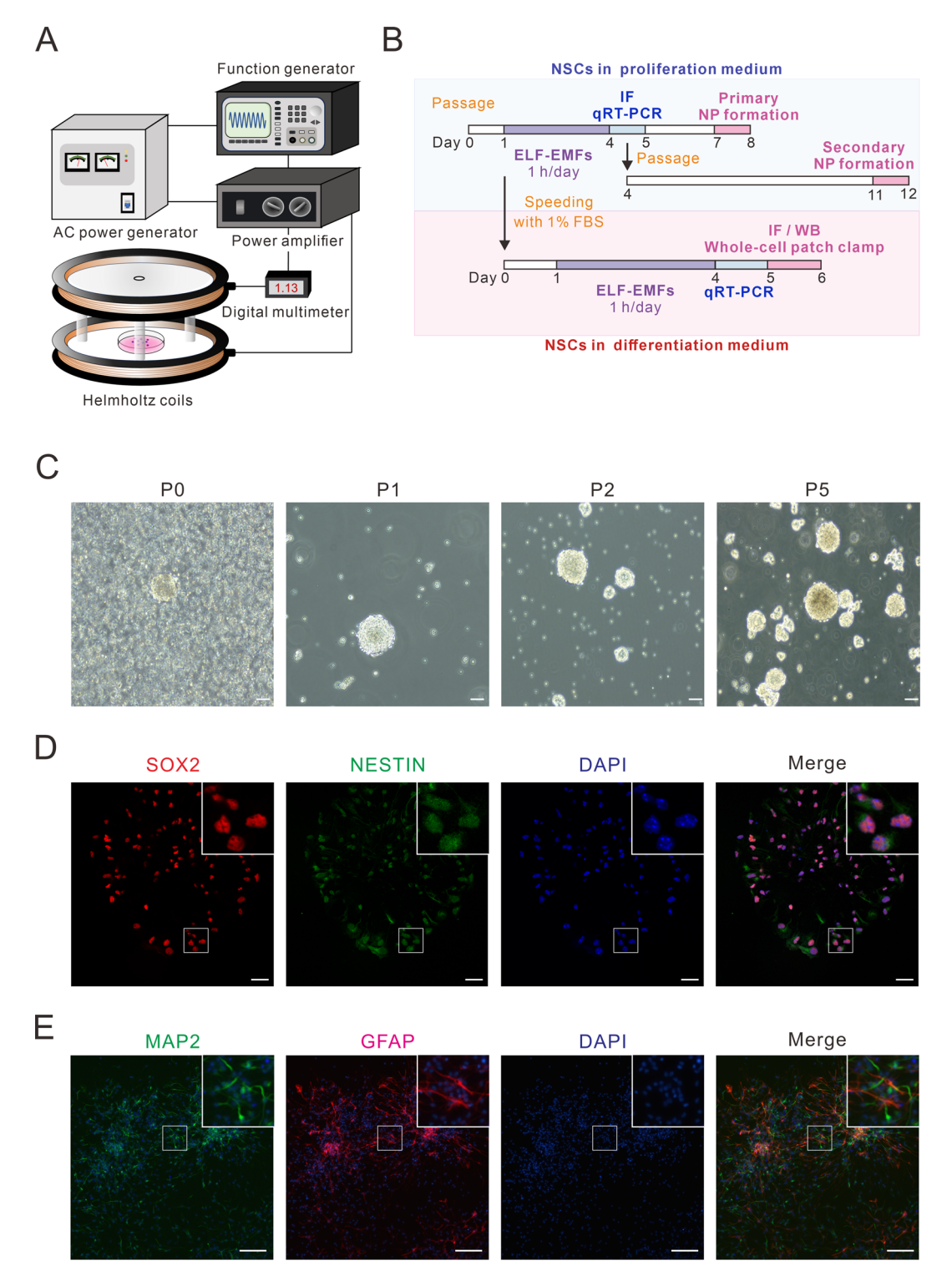


Fig. 1. Experimental design and characterization of the spinal cord-derived NSCs. **A** Schematic of the ELF-EMF system, consisting of a pair of Helmholtz coils powered by an AC generator. **B** Process diagram for the experiment. Spinal cord-derived NSCs cultured in proliferation medium were exposed to ELF-EMFs for 3 days and then processed for immunocytochemical and molecular analyses, as well as NSCs maintenance assays. Following differentiation induction with proliferation medium containing 1% FBS, NSCs were exposed to ELF-EMFs for 3 days and subsequently processed for immunocytochemical and molecular analyses. **C** Cultured spinal cord-derived NSCs at generation 0 (P0, left; n=4). Neurospheres formed by spinal cord-derived NSCs at different passages (P1, middle left; P2, middle right; P5, right; n=4). Scale bar, 100 μm. **D** Representative confocal images showing the colocalization of Sox2 (red), Nestin (green), and DAPI (blue) in neurospheres derived from spinal NSCs (n=5). Scale bar, 25 μm. Insets display magnified view of the boxed region. **E** Immunostaining for MAP2 (green), GFAP (red), and DAPI (blue) in spinal cord-derived NSCs cultured in differentiation medium for 3 days (n=4). Scale bar, 100 μm. Insets display magnified view of the boxed region.

duration of ELF-EMF exposure, as well as air and culture medium temperatures, were continuously monitored. Control groups were kept under the same environmental conditions but without ELF-EMF exposure. Based on previous studies³³, three different intensities (0.2, 0.5, and 1 mT) were selected, and cells were exposed for 1 h per day for 3 consecutive days (Fig. 1B). Spinal cord-derived NSCs were cultured overnight before being exposed to the ELF-EMFs.

Stimulation was performed in 3D neurosphere conditions to assess the effects of ELF-EMFs on undifferentiated NSCs 34 . Following ELF-EMF exposure, the neurospheres were dissociated into single cells and transferred to 2D adherent conditions for downstream analysis. In the neuronal differentiation assay, NSCs were plated in 2D adherent culture prior to ELF-EMF stimulation to ensure controlled differentiation and reproducible analysis.

Cell proliferation assay

Spinal cord-derived NSCs were cultured in $25~\text{cm}^2$ flasks and exposed to ELF-EMFs at varying intensities for 3 consecutive days. Twenty-four hours after the final exposure, cells were collected, dissociated, and 1.0×10^5 cells were seeded on PDL-coated glass coverslips in 24-well plates. After 4 h of attachment, cells were stained for Ki67 using immunofluorescence.

Neurosphere assays

The neurosphere assays include the neurosphere forming assay (primary NP formation) and the self-renewal assay (secondary NP formation), as previously described 35,36 . For the primary NP formation assay, single NSCs (1,000 cells in 200 µl proliferation medium) were seeded into a 96-well plate and exposed to ELF-EMFs for 3 consecutive days. Following an additional 4 days of culture, neurospheres were identified and quantified in accordance with strict morphological criteria: phase-bright and spherical structures ($100-500 \, \mu m$ in diameter) with surface micro-spikes 37 . For the secondary NP formation assay, spinal cord-derived NSCs were cultured in proliferation medium and exposed to ELF-EMFs for 3 consecutive days. The newly formed neurospheres were then collected, dissociated into single cells, and seeded into 96-well plates ($1,000 \, cells$ in $200 \, \mu$ l proliferation medium) without further ELF-EMF exposure. After 7 days of culture, secondary neurospheres were counted using the same stringent morphological criteria. All counts were performed using an inverted microscope (CKX53, Olympus, Japan) at $10 \times magnification$, with data expressed as the mean number of neurospheres per $1,000 \, seeded$ cells from $\geq 3 \, biological$ replicates.

Immunofluorescent histochemistry

Cells cultured on PDL-coated coverlips were washed twice with PBS and fixed with 4% paraformaldehyde for 15 min. The cells were then permeabilized with 0.5% Triton X-100 in PBS for 30 min at room temperature and blocked with 10% goat serum for 30 min. Coverslips were incubated with primary antibodies (see Table 1) at 4°C for 24 h, followed by fluorescently conjugated secondary antibodies (Alexa Fluor 488-labelled goat-anti-chicken, Abcam, USA; Alexa Fluor 488-labelled goat anti-mouse, Beyotime Biotechnology, China; Cy3-labeled goat antirabbit, Beyotime Biotechnology, China) at room temperature for 1 h. DAPI (Invitrogen, USA) was used to stain the fixed cell nucleus. Cells were counted in 4 different fields of each coverslip using a confocal fluorescence microscope (LSM 700, ZEISS, Germany). The morphometry and the length of neurites were semi-automatically characterized by NeuronJ (ImageJ plugin, ver 1.4.3) according to previous studies 38,39.

Western blot analysis

Cells cultured on PDL-coated coverlips were lysed using radioimmunoprecipitation assay (RIPA) lysis buffer (Beyotime Biotechnology, China) supplemented with a protease inhibitor cocktail (Selleck, USA). Protein concentrations were determined via bicinchoninic acid (BCA) assay (Beyotime Biotechnology, China). Protein samples were resolved on 10% SDS-PAGE and transferred to PVDF membranes (Millipore, Germany) using transfer buffer (25 mM Tris, 192 mM glycine, 20% methanol) for 90 min at 200 mA. Membranes were blocked with TBS-T (20 mM Tris-HCl adjusted to pH 7.4, 500 mM NaCl, and 0.1% Tween 20) containing 5% non-

Target	Source	Company	Catalog number	Use
Sox2	Rabbit	Abcam	ab97959	IF
Nestin	Mouse	Abcam	ab6142	IF
MAP2	Chicken	Abcam	ab5392	IF
Ki67	Rabbit	Abcam	ab15580	IF
Tuj1	Mouse	Abcam	ab78078	IF
NeuN	Rabbit	Abcam	ab177487	IF, WB
GFAP	Rabbit	Abcam	ab7260	IF, WB
NeuroD1	Mouse	Proteintech	12081-1-AP	WB
NeuroG1	Rabbit	Proteintech	66642-1-Ig	WB
Cav3.1	Rabbit	Invitrogen	PA5-37236	WB
Cav3.2	Rabbit	Invitrogen	PA5-72836	WB
Cav3.3	Rabbit	Invitrogen	PA1-12666	WB
β-actin	Mouse	Proteintech	66009-1-Ig	WB

Table 1. Primary antibodies used in this study.

fat milk at room temperature for 1 h, then probed with specific primary antibodies (see Table 1) overnight at 4 °C. β -actin was used as an internal reference. Membranes were incubated with horseradish peroxidase (HRP)-conjugated secondary antibodies (Proteintech, 1 : 5000 in TBS-T with 5% non-fat milk) at room temperature for 1 h. After a final wash with TBS-T, bands were detected by enhanced chemiluminescence (ECL) reagent (Beyotime Biotechnology, China) using an e-Blot Tough Imager (e-Blot, China) following the manufacturer's instructions. For quantitative analysis, the density of the target bands was quantified using ImageJ software (1.51j8, NIH, USA).

Quantitative real-time PCR

Total RNA was extracted from cells using TRIzol reagent (Takara, Japan). RNA concentrations were measured using a NanoDrop 2000 spectrophotometer (Thermo Fisher, USA), with an ${\rm OD_{260}/OD_{280}}$ ratio of approximately 2.0. cDNAs were synthesized from 0.5 μ g of total RNA using the Transcriptor First Strand cDNA Synthesis Kit (Takara, Japan). Target mRNA levels were quantified via quantitative real-time PCR (qRT-PCR) using SYBR Green Supermix (Bio-Rad, USA) and normalized to GAPDH expression. The specific primers used for qRT-PCR are listed in Table 2.

Whole-cell patch clamp recordings

Whole-cell patch clamp recordings were conducted to examine Ca^{2+} currents, as described previously³⁹. The extracellular solution contained (in mM): 144 tetraethylammonium (TEA)-MeSO₃, 10 HEPES, and 1.8 CaCl₂, with the pH adjusted to 7.4 using TEA-OH and osmolarity adjusted to 300–310 mOsm with glucose. Recording pipettes (resistance: 4–6 M Ω) were filled with intracellular solution (pH 7.3, adjusted with CsOH) containing (in mM): 138 Cs-MeSO₃, 5 CsCl, 0.5 EGTA, 10 HEPES, 1 MgCl₂, and 2 mg/ml Mg-ATP. To block T-type calcium channels, cells were exposed to 2 μ M TTA-P2 for at least 5 min prior to recording⁴⁰. Drug application was performed using a gravity-driven perfusion system (VC-6, Warner Instruments) with a flow rate of 2 ml/min, allowing complete solution exchange within 30 s. Following the recording of TTA-P2 effects, a 10-minute washout with TTA-P2-free extracellular solution was conducted to assess reversibility.

Cells were clamped at -70 mV with series resistance compensated by 80%. Recordings were excluded if series resistance exceeded 15 M Ω . Leak currents were subtracted using an online P/4 protocol. Ca²⁺ currents were recorded by depolarizing membrane potentials from -70 to +40 mV in 10 mV increments for 100 ms. Data were obtained using an Axopatch 1550B amplifier (Molecular Device, USA), filtered at 2 kHz, and sampled at 10 kHz.

Data analysis

All data are presented as mean ± SEM (standard error of the mean) from at least 3 independent experiments performed in duplicate, unless otherwise specified. For Gaussian-distributed data, statistical significance was determined using one-way ANOVA with Dunnett's or Tukey's *post-hoc* test. All statistical analyses were performed using GraphPad Prism (version 10.1.2, GraphPad Software, USA) or Igor Pro (version 9.0.5, WaveMetrics, USA). A p-value < 0.05 was considered statistically significant.

Results

Identification of the spinal cord-derived neural stem cells

NPCs were derived from the spinal cords of 8-week-old C57BL/6 mice, following previously published protocols³¹. After generating a single-cell suspension, the cells were resuspended in proliferation medium for 10 days, leading to the formation of neurospheres (Fig. 1C, left). These neurospheres exhibited self-renewal capacity, as demonstrated by their ability to undergo further subculturing (Fig. 1C). To confirm the identity of the neurospheres, we employed the NSC markers Sox2 and Nestin. Immunostaining showed that the neurospheres were positive for Nestin and Sox2, with the two markers colocalized (Fig. 1D), confirming the presence of NSCs.

Gene	Forward primer	Reverse primer	
Sox2	5'-AACCGATGCACCGCTACGA-3'	5'-TGCTGCGAGTAGGACATGCTG-3'	
NeuN	5'-CCACGCTTCTCCTTGTCTCG-3'	5'-CCTTGAAGCCAGCATTGAGC-3'	
NeuroD1	5'-ACAACAGGAAGTGGAAACATGACC-3'	5'-CACTCATCTGTCCAGCTTGGG-3'	
NeuroD2	5'-CCAAGCCAGTGTCTCTTC-3'	5'-CTTCCTCCTCCTCTCT.3'	
NeuroG1	5'-CCAGCGACACTGAGTCCTG-3'	5'-CGGGCCATAGGTGAAGTCTT-3'	
NeuroG2	5'-GTCATCCTCCAACTCCACGTC-3'	5'-AGGCGCATAACGATGCTTCTC-3'	
Cav1.2	5'- CGCAGCGTAAGGATGAGTGA-3'	5'- ACCTAGAGAGGCAGAGCGAA-3'	
Cav1.3	5'- GCTCCCACCTCAACAAATGC-3'	5'- TGCTTGCAGGAGTAATGCCC-3'	
Cav3.1	5'- GCTCTACTTCATCTCCTTCC-3'	5'- GCTTCTCCTTACTCCTTCTC-3'	
Cav3.2	5'- GCTCTTCATCTTCATCTTCAG-3'	5'- AACCACATTCCAGTCTTCC-3'	
Cav3.3	5'- GCACTACAACCAGCCTAC-3'	5'- GACAGACAGCACAAT-3'	
GFAP	5'-AGCCAAGCAGCCCACCAAAC-3'	5'-TCTATACGCAGCCAGGTTGTTCTC-3'	
GAPDH	5'-ATACGGCTACAGCAACAGGG-3'	5'-GCCTCTCTTGCTCAGTGTCC-3'	

Table 2. Primers used in qRT-PCR analyses.

In the context of SCI repair, current research and therapeutic strategies primarily emphasize neuronal regeneration and modulation of astrocytic scarring⁴¹. To examine the lineage-specific differentiation potential of NSCs toward neurons and astrocytes, dissociated neurospheres were cultured in differentiation medium supplemented with 1% FBS for 3 days, followed by immunostaining for MAP2 and GFAP. MAP2 is specifically localized to dendrites and is critical for microtubule stabilization and neurite extension in post-mitotic neurons⁴². Its expression has been widely validated across various in vitro neuronal differentiation models and serves as a robust indicator of neuronal identity. GFAP is the principal intermediate filament protein in astrocytes, serving as an astrocyte-specific marker⁴³. After differentiation for 3 days, we observed MAP2* and GFAP* cells, which were biologically exclusive and not co-expressed in the same cell (Fig. 1E). The observed GFAP* and MAP2* cells represent early lineage commitment rather than terminal maturation^{43,44}, indicative of initial fate specification at this early differentiation stage. These results collectively demonstrate that spinal cord-derived NSCs possess the essential characteristics of self-renewal and differentiation into both neurons and astrocytes, which are fundamental properties of NSCs.

ELF-EMFs promote proliferation and self-renewal of spinal cord-derived neural stem cells

To investigate the effects of ELF-EMFs on the proliferation of spinal cord-derived NSCs, cells were exposed to ELF-EMFs at varying intensities (0.2, 0.5, and 1 mT) for 1 h per day over 3 consecutive days (Fig. 1B). The control group was maintained under identical conditions without ELF-EMF exposure (0 mT). Following treatment, the expression of the proliferation marker Ki67 in NSCs was assessed via immunofluorescence staining. A significant increase in the proportion of Ki67⁺ cells was observed in the ELF-EMF-treated groups compared to the controls (0 mT: $100.0\pm1.8\%$; 0.2 mT: $137.8\pm7.6\%$, p=0.048; 0.5 mT: $148.7\pm13.0\%$, p=0.012; 1 mT: $201.7\pm12.6\%$, p<0.001; n=4; one-way ANOVA with Dunnett's *post-hoc* test; Fig. 2A, B), indicating that ELF-EMF exposure promotes the proliferation of spinal cord-derived NSCs.

To investigate whether ELF-EMFs influence the self-renewal of spinal cord-derived NSCs, we performed a neurosphere formation assay. NSCs were digested into single cells and exposed to ELF-EMFs at different intensities (0.2, 0.5, and 1 mT) for 1 h per day over 3 consecutive days. Following exposure, cells were cultured for an additional 4 days to assess the primary neurosphere formation rate (Fig. 1B). The results showed a significant increase in neurosphere formation after ELF-EMF exposure (0 mT: $100.0\pm6.2\%$; 0.2 mT: $176.2\pm8.1\%$, p=0.047; 0.5 mT: $212.2\pm18.1\%$, p=0.005; 1 mT: $271.8\pm33.7\%$ p<0.001; n=4; one-way ANOVA with Dunnett's *post-hoc* test; Fig. 2C, E), indicating that ELF-EMFs facilitate neurosphere formation in spinal cord-derived NSCs. To assess the maintenance of NSC self-renewal after ELF-EMF exposure, we conducted secondary neurosphere formation analysis. After 3 days of ELF-EMF treatment, newly formed neurospheres were digested into single cells and subcultured for another 7 days to evaluate secondary neurosphere formation (Fig. 1B). The secondary neurosphere formation rate was significantly higher than the control group at 0.5 and 1 mT (0 mT: $100.0\pm5.2\%$; 0.2 mT: $131.8\pm12.9\%$, p=0.225; 0.5 mT: $191.6\pm12.5\%$, p<0.001; 1 mT: $215.7\pm16.8\%$, p<0.001; n=4; one-way ANOVA with Dunnett's *post-hoc* test; Fig. 2D, F).

To explore the underlying cellular mechanisms, we extracted RNA from spinal cord-derived NSCs after ELF-EMF exposure and examined the mRNA levels of Sox2 using qRT-PCR. Sox2 is a well-established master regulator of NSC proliferation and self-renewal⁴⁵. The mRNA levels of Sox2 were significantly upregulated following ELF-EMF exposure (0 mT: $100.0\pm3.3\%$; 0.2 mT: $167.5\pm12.6\%$, p=0.048; 0.5 mT: $189.3\pm23.9\%$, p=0.009; 1 mT: $264.6\pm24.4\%$, p<0.001; n=5; one-way ANOVA with Dunnett's *post-hoc* test; Fig. 2G). The upregulation of Sox2 combined with functional assays, such as increased Ki67* cells and enhanced neurosphere formation, suggest that ELF-EMFs enhance and sustain the self-renewal capacity of spinal cord-derived NSCs.

ELF-EMFs facilitate the differentiation of spinal cord-derived neural stem cells into neurons

To facilitate the process of SCI repair, transplanted NSCs must differentiate into neurons or glial cells, as well as form new synaptic connections and neural circuits. Therefore, we investigated the effects of ELF-EMFs on regulating the differentiation ability of spinal cord-derived NSCs into neurons and glial cells. First, we investigated how ELF-EMFs affect neuronal differentiation.

NSCs were induced to differentiate in medium containing 1% FBS and exposed to ELF-EMFs at varying intensities (0.2, 0.5, and 1 mT) for 1 h per day over 3 consecutive days (Fig. 1B). After 3 days, RNA was extracted, and the expression levels of NeuN, a neuron-specific gene, were quantified using qRT-PCR. The results showed that NeuN mRNA levels increased in a dose-dependent manner following ELF-EMF exposure (0 mT, $100.0 \pm 6.4\%$; 0.2 mT: $168.5 \pm 19.1\%$; 0.5 mT: $299.3 \pm 22.7\%$; 1 mT: $321.8 \pm 21.0\%$; 0 mT vs. 0.2 mT, p = 0.078; 0 mT vs. 0.5 mT, p < 0.001; 0 mT vs. 1 mT, p < 0.001; 0.2 mT vs. 0.5 mT, p < 0.001; 0.2 mT vs. 1 mT, p < 0.001; 0.5 mT vs. 1 mT, p = 0.824; n = 5; one-way ANOVA with Tukey's post-hoc test; Fig. 3C), suggesting that ELF-EMFs facilitate NSCs differentiation into neurons. To further validate this, cells were exposed to ELF-EMFs for 3 days and then immunostained for NeuN (Fig. 3A). The results confirmed that ELF-EMFs facilitate NSCs differentiation into neurons at 0.2 and 0.5 mT (0 mT: 100.0±3.2%; 0.2 mT: 157.1±14.3%; 0.5 mT: 182.0±10.9%; 0 mT vs. 0.2 mT, p = 0.027; 0 mT vs. 0.5 mT, p = 0.002; n = 4; one-way ANOVA with Tukey's post-hoc test; Fig. 3B). The facilitative effect was slightly reduced at 1 mT ($147.2 \pm 16.0\%$; n = 4; 0 mT vs. 1 mT, p = 0.073; Fig. 3B), but was not statistically significant compared to 0.2 and 0.5 mT (0.2 mT vs. 1 mT, p = 0.937; 0.5 mT vs. 1 mT, p = 0.231). Consistent results were obtained from western blot analysis. After 3 days of ELF-EMF exposure, NeuN protein expression was elevated at 0.2 and 0.5 mT (0 mT: $100.0 \pm 8.1\%$; 0.2 mT: $141.2 \pm 5.4\%$; 0.5 mT: $150.9 \pm 10.7\%$; 0 mT vs. 0.2 mT, p = 0.012; 0 mT vs. 0.5 mT, p = 0.002; n = 5; one-way ANOVA with Tukey's post-hoc test; Fig. 3D, E), while the increase was less pronounced at 1 mT (133.5 \pm 7.3%; n = 5; 0 mT vs. 1 mT, p = 0.044; Fig. 3D, E) and not statistically significant compared to 0.2 and 0.5 mT (0.2 mT vs. 1 mT, p = 0.908; 0.5 mT vs. 1 mT, p = 0.454), aligning with the immunostaining data.

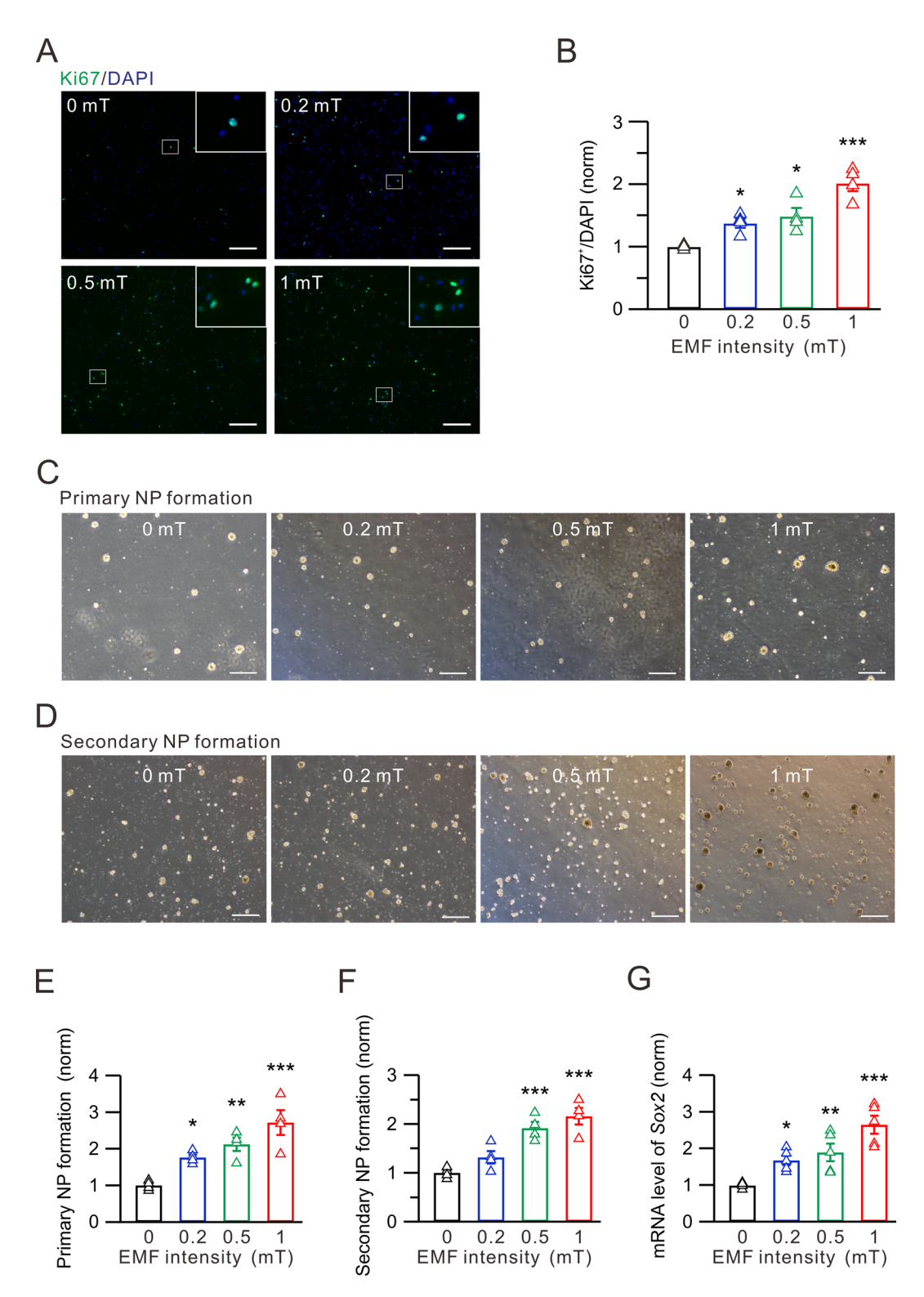
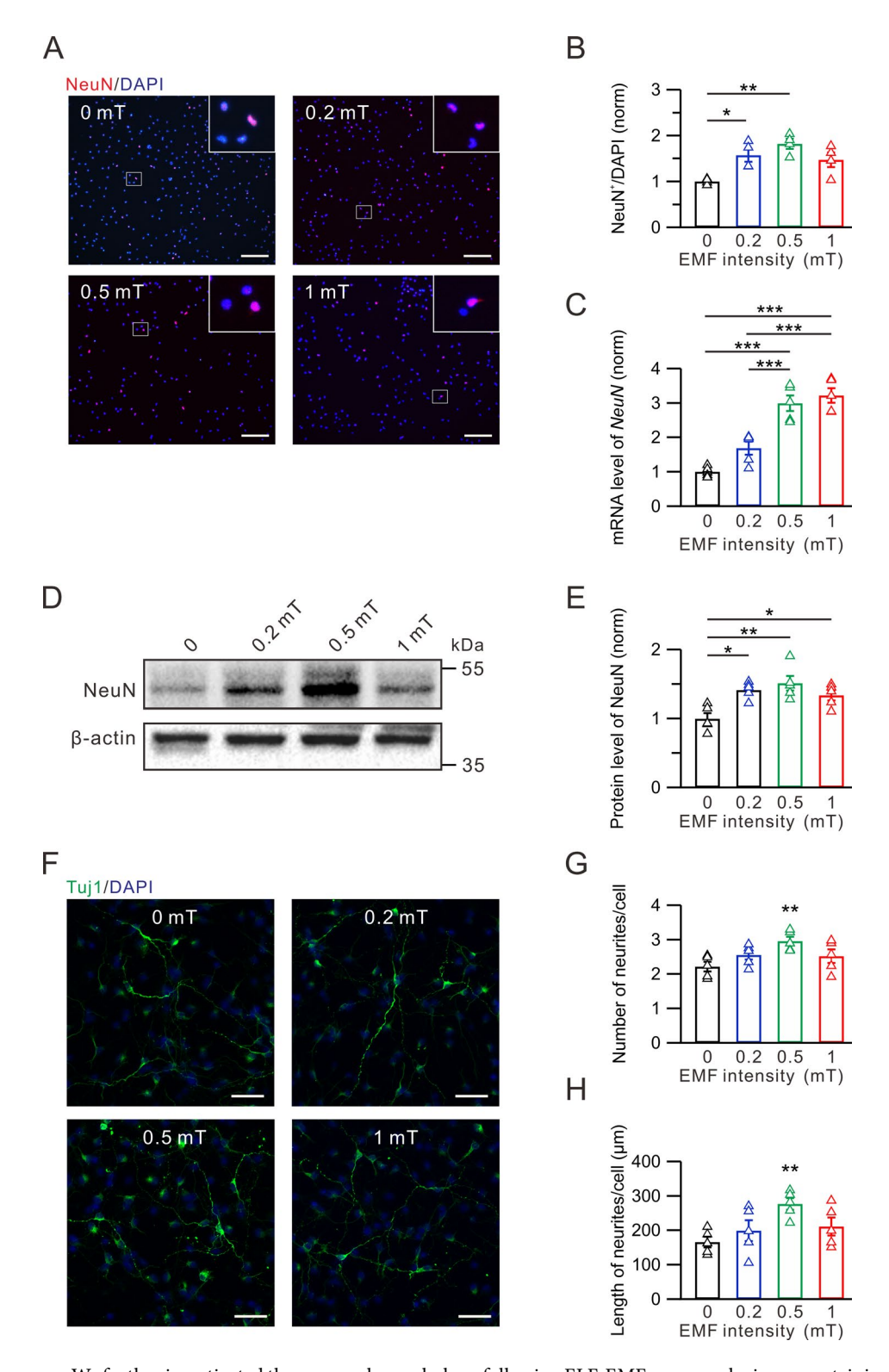


Fig. 2. ELF-EMFs enhance proliferation and self-renewal of spinal cord-derived NSCs. **A** Representative confocal images showing the proliferation of the spinal cord-derived NSCs stained with Ki67 (green) after exposure to ELF-EMFs at different intensities. Scale bar, 100 μm. Insets display magnified view of the boxed region. **B** Quantification of Ki67⁺ cell proportion (n=4). Values are normalized to the 0 mT control group. **C**, **D** Representative images showing self-renewal through primary and secondary neurosphere formation assays after exposure to ELF-EMFs at different intensities. Scale bar, 100 μm. **E**, **F** Quantification of the primary (n=4) and secondary (n=4) neurosphere formation rates. Values are normalized to the 0 mT control group. **G** Quantification of Sox2 mRNA levels in spinal cord-derived NSCs after exposure to ELF-EMFs at different intensities (n=5). Values are normalized to the 0 mT control group.



We further investigated the neuronal morphology following ELF-EMF exposure by immunostaining for Tuj1 (neuron-specific class III β -tubulin) to measure neurite number and length. After ELF-EMF exposure, both the number and length of neurites per cell significantly increased at 0.5 mT (number: 2.96 ± 0.13 , p=0.009, n=5; length: 276.2 ± 16.9 µm, p=0.009, n=5; one-way ANOVA with Dunnett's *post-hoc* test; Fig, 3F-H). Increases at 0.2 and 1 mT were not statistically significant (number: 0 mT, 2.21 ± 0.14 ; 0.2 mT, 2.56 ± 0.14 , p=0.295; 1 mT, 2.52 ± 0.20 , p=0.380; n=5; length: 0 mT, 165.6 ± 15.3 µm; 0.2 mT, 198.9 ± 30.1 µm, p=0.614; 1 mT, 210.7 ± 25.8 µm, p=0.390; n=5; one-way ANOVA with Dunnett's *post-hoc* test; Fig. 3F-H). These findings suggest that ELF-EMFs facilitate neurite outgrowth at 0.5 mT, potentially enhancing synaptic connections and neuronal network development.

∢Fig. 3. ELF-EMFs facilitate differentiation of spinal cord-derived NSCs into neurons. **A** Representative confocal images showing immunostaining for NeuN after exposure to ELF-EMFs at different intensities. Scale bar, 100 μm. Insets display magnified view of the boxed region. **B** Quantification of NeuN⁺ cells after exposure to ELF-EMFs at different intensities (*n* = 4). Values are normalized to the 0 mT control group. **C** Quantification of *NeuN* mRNA levels after exposure to ELF-EMFs at different intensities (*n* = 5). Values are normalized to the 0 mT control group. **D** Protein levels of *NeuN* in spinal cord-derived NSCs after exposure to ELF-EMFs at different intensities, with β-actin used as a loading control. Original blots are presented in Supplementary Fig. 1A. **E** Quantification of *NeuN* protein levels after exposure to ELF-EMFs at different intensities (*n* = 5). Values are normalized to the 0 mT control group. **F** Representative confocal images stained with Tuj1, showing neurites growth after exposure to ELF-EMFs at different intensities. Scale bar, 50 μm. **G** Quantification of the number of neurites per cell after exposure to ELF-EMFs at different intensities (*n* = 5). **H** Statistics for neurite length per cell after exposure to ELF-EMFs at different intensities (*n* = 5).

ELF-EMFs activate pro-neuronal genes and T-type calcium channels

Previous studies have identified key transcription factors of the basic Helix-Loop-Helix (bHLH) family, including Neurogenin1/2 (NeuroG1/2) and Neurogenic Differentiation 1/2 (NeuroD1/2), as critical regulators of neurogenesis^{46,47}. To explore the mechanisms underlying ELF-EMF-induced NSCs differentiation, we assessed the mRNA levels of NeuroD1, NeuroD2, NeuroG1, and NeuroG2 using qRT-PCR. The results showed that ELF-EMF exposure significantly increased the mRNA levels of NeuroD1 and NeuroG1 (Fig. 4A; Table 3), while the mRNA expression of NeuroD2 and NeuroG2 remained unaffected (Fig. 4B; Table 3). Western blot analysis further confirmed increased protein levels of NeuroD1 and NeuroG1 after 3 days of ELF-EMF exposure (Fig. 4C, D; Table 3). These results indicate that ELF-EMFs may facilitate NSC differentiation into neurons by upregulating pro-neuronal gene expression such as NeuroD1 and NeuroG1.

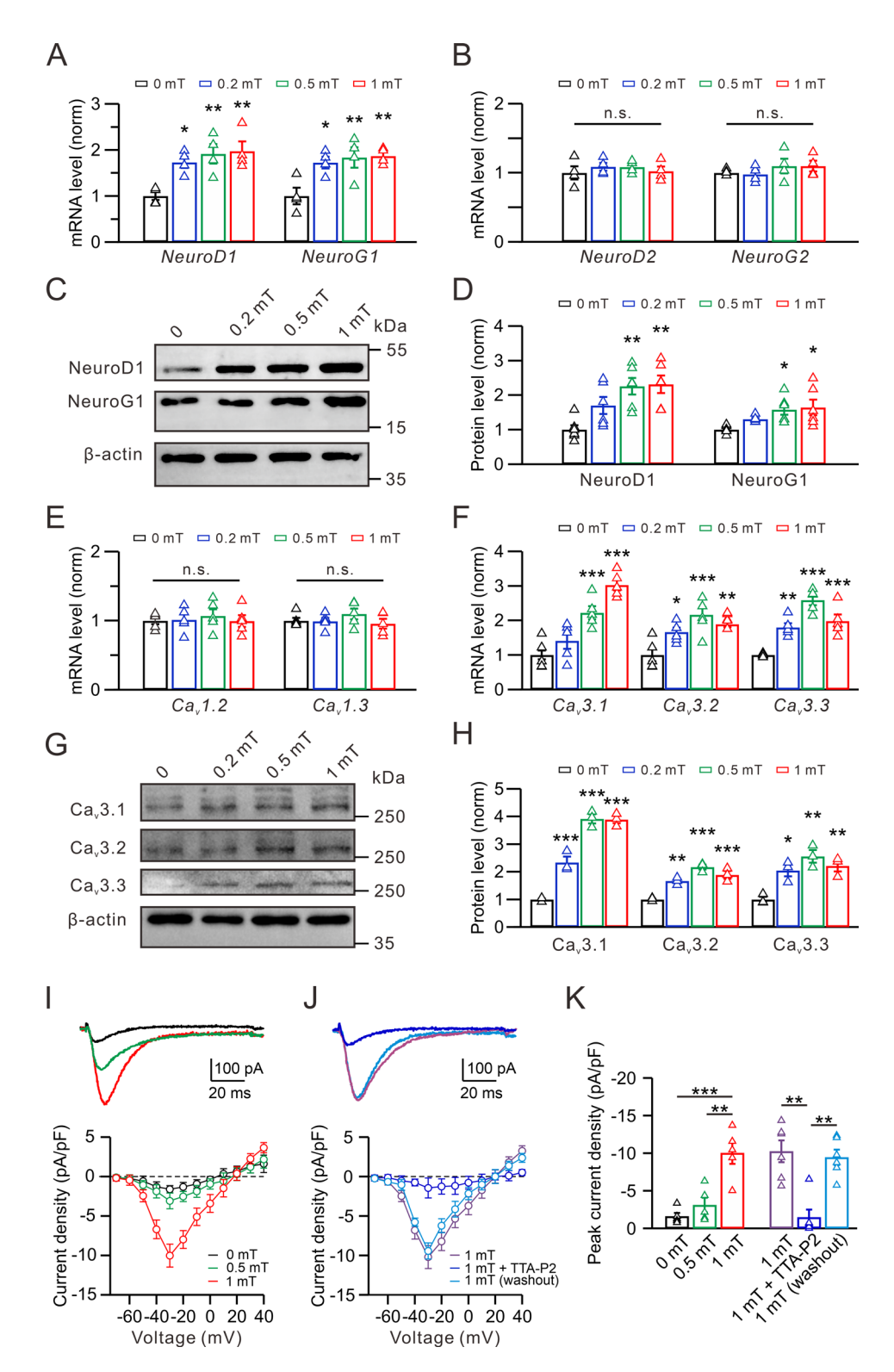
Voltage-gated calcium channels (VGCCs) are key mediators of intracellular signaling and have been proposed to be influenced by ELF-EMFs⁴⁸. Previous studies have shown that calcium influx through VGCC, particularly L- and T-type calcium channels, regulates signaling pathways involved in cell proliferation, programmed cell death, and neuronal differentiation in NSCs^{48–50}. To investigate the impact of ELF-EMFs on VGCCs in NSCs, we examined the expression of L- and T-type calcium channels using qRT-PCR. After ELF-EMF exposure, mRNA levels of L-type calcium channels ($Ca_v 1.2$ and $Ca_v 1.3$) showed no significant changes (Fig. 4E; Table 3). However, T-type calcium channel ($Ca_v 3.1$, $Ca_v 3.2$, and $Ca_v 3.3$) mRNA levels significantly increased after ELF-EMF exposure (Fig. 4F; Table 3). Western blot analyses further confirmed these findings, showing increased T-type calcium channel protein levels (Fig. 4G, H; Table 3).

To assess the functional activity of calcium channels after ELF-EMF exposure, we recorded calcium currents using whole-cell patch clamp recordings and plotted the current density-voltage (I-V) curve. Whole-cell patch clamp recordings were conducted on day 2 after the final ELF-EMF exposure (Fig. 1B). At this stage, cells had been cultured in differentiation medium for 6 days, exhibiting initial neuronal characteristics. Maximal calcium currents were observed at -30 mV (Fig. 4I), indicating that T-type calcium channels are the predominant VGCCs in NSCs⁵¹. After 3 days of ELF-EMF exposure, calcium currents increased significantly without a shift in peak voltage (-30 mV: 0 mT, -1.61 ± 0.45 pA/pF; 0.5 mT, -3.09 ± 0.98 pA/pF; 1 mT, -10.03 ± 1.44 pA/pF; 0 mT vs. 0.5 mT, p=0.588; 0 mT vs. 1 mT, p<0.001; 0.5 mT vs. 1 mT, p=0.001; n=5; one-way ANOVA with Tukey's post-hoc test; Fig. 4I, K). This increase was substantially inhibited by 2 μ M TTA-P2, a specific T-type calcium channel blocker (-30 mV: 1 mT, -10.23 ± 1.45 pA/pF; 1 mT + TTA-P2, -1.45 ± 1.02 pA/pF; 1 mT [washout], -9.44 ± 1.02 pA/pF; 1 mT vs. 1 mT, TTA-P2, p=0.004; 1 mT vs. 1 mT [washout], p=0.878; 1 mT + TTA-P2 vs. 1 mT [washout], p=0.878; 1 mT + TTA-P2 vs. 1 mT [washout], p=0.878; 1 mT + TTA-P2 vs. 1 mT [washout], p=0.878; 1 mT + TTA-P2 vs. 1 mT [washout], p=0.878; 1 mT + TTA-P2 vs. 1 mT [washout], p=0.878; 1 mT + TTA-P2 vs. 1 mT [washout], p=0.878; 1 mT + TTA-P2 vs. 1 mT [washout], p=0.878; 1 mT + TTA-P2 vs. 1 mT [washout], p=0.878; 1 mT + TTA-P2 vs. 1 mT [washout], p=0.878; 1 mT + TTA-P2 vs. 1 mT [washout], p=0.878; 1 mT + TTA-P2 vs. 1 mT [washout], p=0.878; 1 mT + TTA-P2 vs. 1 mT [washout], p=0.878; 1 mT + TTA-P2 vs. 1 mT [washout], p=0.878; 1 mT + TTA-P2 vs. 1 mT [washout], p=0.878; 1 mT + TTA-P2 vs. 1 mT [washout], p=0.878; 1 mT + TTA-P2 vs. 1 mT [washout], p=0.878; 1 mT + TTA-P2 vs. 1 mT [washout], p=0.878; 1 mT + TTA-P2 vs. 1 mT [washout], p=0.878; 1 mT + TTA-P2 vs. 1 mT [washout], p=0.878;

ELF-EMFs do not affect the differentiation of spinal cord-derived neural stem cells into astrocytes

Glial cells, including astrocytes, oligodendrocytes, and microglia, are abundant non-neuronal cells in the nervous system that support neuronal migration and contribute to nervous system repair and regeneration⁵². In the injured spinal cord, NSCs largely differentiate into astrocytes, while oligodendrocyte differentiation tends to be limited and typically occurs only in regions with preserved axonal architecture⁵³. To determine whether ELF-EMFs influence astrocytic differentiation, we examined the differentiation of spinal cord-derived NSCs into astrocytes. Astrocytic differentiation was induced using the same protocol as neuronal differentiation, without adding astrocyte-specific cytokines or inducers, allowing for direct comparison of astrocytic and neuronal outcomes.

Immunostaining for GFAP revealed no significant differences in astrocytic differentiation across ELF-EMF intensities from 0.2 to 1 mT (0 mT: $100.0\pm2.9\%$; 0.2 mT: $103.7\pm5.0\%$, p=0.963; 0.5 mT: $109.2\pm10.0\%$, p=0.666; 1 mT: $107.3\pm7.2\%$, p=0.794; n=5; one-way ANOVA with Dunnett's *post-hoc* test; Fig. 5A, B). These findings were corroborated by qRT-PCR and western blot analysis, which showed no significant changes in mRNA (0 mT: $100.0\pm6.7\%$; 0.2 mT: $89.7\pm11.6\%$, p=0.898; 0.5 mT: $92.7\pm13.4\%$, p=0.958; 1 mT: $107.8\pm17.7\%$, p=0.951; n=5; one-way ANOVA with Dunnett's *post-hoc* test; Fig. 5C) or protein levels (0 mT: $100.0\pm10.9\%$; 0.2 mT: $95.8\pm8.6\%$, p=0.991; 0.5 mT, $94.3\pm11.7\%$, p=0.980; 1 mT, $110.8\pm18.8\%$, p=0.889; n=5; one-way ANOVA with Dunnett's *post-hoc* test; Fig. 5D, E), suggesting a negligible effect of ELF-EMFs on astrocytic differentiation from NSCs.



Discussion

The proliferation and differentiation of spinal cord-derived NSCs are essential for maintaining cell populations and generating neuronal diversity during spinal cord development, growth, and repair 4,6,8,9 . The biological effects of electromagnetic fields, particularly ELF-EMFs, have been studied for over 20 years, with substantial evidence supporting their potential influence on various biological systems 54 , including cancer 55 , immune cells 23 , bone cells 56 , and nerve cells 21,57 . Previous studies have shown that ELF-EMF exposure can stimulate cell proliferation across multiple cellular models 58 , including adult brain NSCs 48,59 . However, the effects of ELF-EMFs on the proliferation and differentiation of spinal cord-derived NSCs remain poorly understood, thereby limiting their potential clinical applications in SCI treatment.

In this study, we investigated the effects of ELF-EMFs on the proliferation, self-renewal, and multidirectional differentiation of spinal cord-derived NSCs using assays for cell proliferation, neurospheres formation, cell

▼Fig. 4. ELF-EMFs upregulate the expression of pro-neuronal genes and activate T-type calcium channels. A, **B** Quantification of NeuroD1 (n=4), NeuroG1 (n=4), NeuroG2 (n=4), and NeuroD2 (n=4) mRNA levels in spinal cord-derived NSCs after exposure to ELF-EMFs at different intensities. Values are normalized to the 0 mT control group. C Protein levels of NeuroD1 and NeuroG1 in spinal cord-derived NSCs after exposure to ELF-EMFs at different intensities, with β -actin used as a loading control. Original blots are presented in Supplementary Fig. 1B. D Quantification of NeuroD1 (n=6) and NeuroG1 (n=6) protein levels in spinal cord-derived NSCs after exposure to ELF-EMFs at different intensities. Values are normalized to the 0 mT control group. E, F Quantification of $Ca_{\nu}1.2$ (n=5), $Ca_{\nu}1.3$ (n=5), $Ca_{\nu}3.1$ (n=5), $Ca_{\nu}3.2$ (n=5) and $Ca_{\nu}3.3$ (n = 5) mRNA levels in spinal cord-derived NSCs after exposure to ELF-EMFs at different intensities. Values are normalized to the 0 mT control group. G Protein levels of Ca, 3.1, Ca, 3.2 and Ca, 3.3 in spinal cord-derived NSCs after exposure to ELF-EMFs at different intensities, with β -actin used as a loading control. Original blots are presented in Supplementary Fig. 1C. H Quantification of $Ca_v3.1$ (n=3), $Ca_v3.2$ (n=3) and $Ca_v3.3$ (n=3)protein levels in spinal cord-derived NSCs after exposure to ELF-EMFs at different intensities. Values are normalized to the 0 mT control group. I Representative calcium current traces recorded at -30 mV and current density-voltage (I-V) curves of NSC-differentiated neurons after exposure to ELF-EMFs at different intensities (0 mT, black, n = 5; 0.5 mT, green, n = 5; 1 mT, red, n = 5). J Representative calcium current traces recorded at -30 mV and current density-voltage (I-V) curves in NSC-differentiated neurons at 1 mT (1 mT, purple, n=6; 1 mT + TTA-P2, 1 mT with 2 μ M TTA-P2 in the bath solution, blue, n = 6; 1 mT [washout], after 10-min washout with TTA-P2-free solution, light blue, n = 6). K Statistics for peak current density of NSC-differentiated

Property	0 mT	0.2 mT	0.5 mT	1 mT	Test
NeuroD1 mRNA level (%)	100.0 ± 8.7	173.1 ± 12.3	191.3 ± 21.0	197.5 ± 21.0	0 mT vs. 0.2 mT, * p = 0.024; 0 mT vs. 0.5 mT, ** p = 0.006; 0 mT vs. 1 mT, ** p = 0.004; n = 4
NeuroG1 mRNA level (%)	100.0 ± 17.8	172.7 ± 12.5	183.4 ± 22.0	186.8 ± 8.6	0 mT vs. 0.2 mT, * $p = 0.020$; 0 mT vs. 0.5 mT, ** $p = 0.008$; 0 mT vs. 1 mT, ** $p = 0.007$; $n = 4$
NeuroD2 mRNA level (%)	100.0 ± 9.5	108.5 ± 5.7	108.2 ± 4.5	102.2 ± 6.8	0 mT vs. 0.2 mT, p = 0.716; 0 mT vs. 0.5 mT, p = 0737; 0 mT vs. 1 mT, p = 0.992; n = 4
NeuroG2 mRNA level (%)	100.0 ± 2.1	97.8 ± 5.8	109.6 ± 10.7	109.7 ± 7.7	0 mT vs. 0.2 mT, $p = 0.993$; 0 mT vs. 0.5 mT, $p = 0.680$; 0 mT vs. 1 mT, $p = 0.672$; $n = 4$
NeuroD1 protein level (%)	100.0 ± 12.8	169.7 ± 25.0	225.7 ± 24.2	231.2 ± 25.6	0 mT vs. 0.2 mT, $p = 0.104$; 0 mT vs. 0.5 mT, ** $p = 0.002$; 0 mT vs. 1 mT, ** $p = 0.002$; $n = 6$
NeuroG1 protein level (%)	100.0 ± 4.7	130.8 ± 3.6	157.7 ± 15.1	164.5 ± 22.9	0 mT vs. 0.2 mT, p = 0.315; 0 mT vs. 0.5 mT, * p = 0.024; 0 mT vs. 1 mT, * p = 0.011; n = 6
Ca _v 1.2 mRNA level (%)	100.0 ± 5.0	101.2 ± 7.9	106.9 ± 9.6	99.5 ± 8.6	0 mT vs. 0.2 mT, $p = 0.992$; 0 mT vs. 0.5 mT, $p = 0.871$; 0 mT vs. 1 mT, $p > 0.999$; $n = 5$
Ca _v 1.3 mRNA level (%)	100.0 ± 4.3	99.0 ± 4.9	109.7 ± 7.7	95.7 ± 7.0	0 mT vs. 0.2 mT, p = 0.999; 0 mT vs. 0.5 mT, p = 0.555; 0 mT vs. 1 mT, p = 0.926; n = 5
Ca _v 3.1 mRNA level (%)	100.0 ± 13.0	141.3 ± 23.4	222.4 ± 19.1	302.9 ± 15.5	0 mT vs. 0.2 mT, $p = 0.287$; 0 mT vs. 0.5 mT, *** $p < 0.001$; 0 mT vs. 1 mT, *** $p < 0.001$; $n = 5$
Ca _v 3.2 mRNA level (%)	100.0 ± 18.5	162.5 ± 12.6	210.0 ± 22.1	203.7 ± 8.2	0 mT vs. 0.2 mT, * p = 0.039; 0 mT vs. 0.5 mT, *** p < 0.001; 0 mT vs. 1 mT, ** p = 0.001; n = 5
Ca _v 3.3 mRNA level (%)	100.0 ± 1.9	180.1 ± 12.1	258.9 ± 14.5	198.2 ± 18.9	0 mT vs. 0.2 mT, *** $p = 0.002$; 0 mT vs. 0.5 mT, *** $p < 0.001$; 0 mT vs. 1 mT, *** $p < 0.001$; $n = 5$
Ca _v 3.1 protein level (%)	100.0 ± 4.2	233.8 ± 20.8	391.8 ± 16.6	388.8 ± 13.4	0 mT vs. 0.2 mT, *** p < 0.001; 0 mT vs. 0.5 mT, *** p < 0.001; 0 mT vs. 1 mT, *** p < 0.001; n = 3
Ca _v 3.2 protein level (%)	100.0 ± 3.6	166.5 ± 7.5	216.8 ± 9.2	188.8 ± 13.7	0 mT vs. 0.2 mT, *** $p = 0.002$; 0 mT vs. 0.5 mT, *** $p < 0.001$; 0 mT vs. 1 mT, *** $p < 0.001$; $n = 3$
Ca _v 3.3 protein level (%)	100.0 ± 10.0	204.3 ± 21.5	255.8 ± 22.9	221.4 ± 20.2	0 mT vs. 0.2 mT, * $p = 0.013$; 0 mT vs. 0.5 mT, ** $p = 0.001$; 0 mT vs. 1 mT, ** $p = 0.006$; $n = 3$

Table 3. Transcription and expression levels of specific genes in NSCs from treated and untreated groups. Each value is presented as the mean \pm SEM. Statistical analysis was performed using one-way ANOVA with Dunnett's *post-hoc* test.

differentiation, neurite analysis, and calcium channel activities. Our findings demonstrate that ELF-EMFs enhance NSC proliferation and self-renewal by upregulating Sox2 expression (Fig. 2). Furthermore, ELF-EMFs significantly promoted neuronal differentiation and increased neurite outgrowth by enhancing T-type calcium channel activity and upregulating pro-neuronal genes NeuroD1 and NeuroG1 (Figs. 3 and 4). However, no significant effect was observed on astrocytic differentiation (Fig. 5).

Previous studies have reported varied effects of ELF-EMFs on neuronal differentiation, with some showing no impact on embryonic NSCs under intermittent exposure^{60,} while others demonstrated enhanced neuronal differentiation in postnatal and adult NSCs under different exposure durations^{34,48}. Our results show that consistent ELF-EMF exposure (0.2, 0.5, and 1.0 mT, 1 h per day for 3 days) significantly increased the proportion of neurons differentiated from spinal cord-derived NSCs (Fig. 3), suggesting that both magnetic field intensity and exposure duration may influence neuronal differentiation. Interestingly, we found that ELF-EMFs did not affect the proportion of NSCs differentiating into astrocytes (Fig. 5), while Isakovic et al. reported that ELF-EMFs steer the differentiation of embryonic NSCs towards astrocyte-like phenotypes¹⁸. These findings indicate a selective effect of ELF-EMFs on neuronal lineage development. And this specificity warrants further in vivo investigation to determine whether ELF-EMFs promote spinal cord-derived NSC differentiation preferentially towards neurons or glial cells.

Consistent with the protocol outlined in Fig. 1B, NSCs were collected on day 4 for *NeuN* mRNA assessment via qRT-PCR immediately after the final ELF-EMF exposure, or on day 5 for *NeuN* protein detection via immunostaining. We observed that the mRNA levels of *NeuN* increased in a dose-dependent manner with the intensity of ELF-EMFs (Fig. 3C). However, by day 5, the proportion of neurons in the 0.2 and 0.5 mT groups remained significantly elevated compared to control, while the proportion in the 1.0 mT group showed

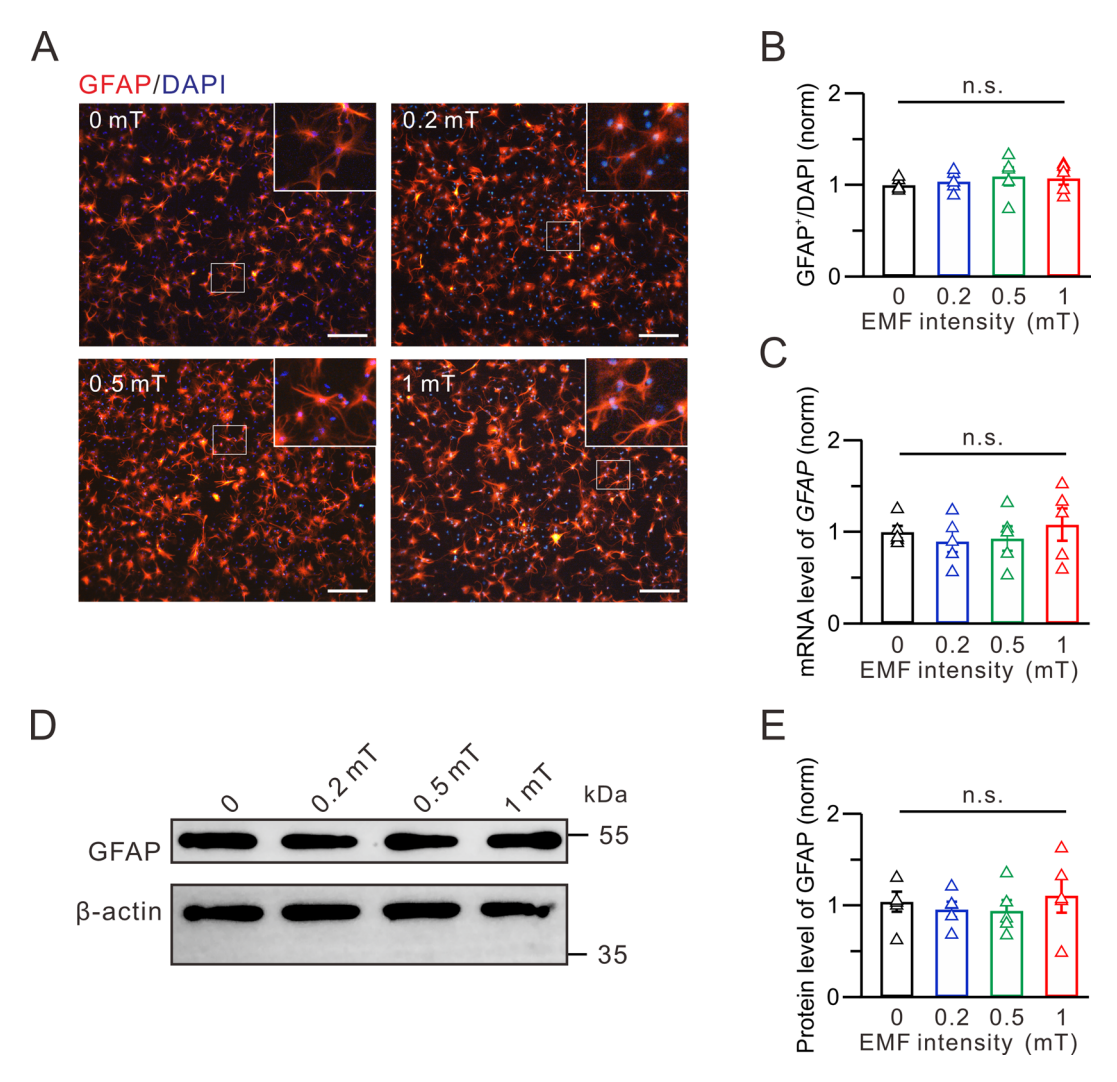


Fig. 5. ELF-EMFs have no impact on astrocytic differentiation. **A** Representative confocal images showing GFAP immunostaining after exposure to ELF-EMFs at different intensities. Scale bar, 100 μm. Insets display magnified view of the boxed region. **B** Quantification of GFAP⁺ cells after exposure to ELF-EMFs at different intensities (n = 5). Values are normalized to the 0 mT control group. **C** Quantification of *GFAP* mRNA levels in spinal cord-derived NSCs after exposure to ELF-EMFs at different intensities (n = 5). Values are normalized to the 0 mT control group. **D** Protein levels of *GFAP* in spinal cord-derived NSCs after exposure to ELF-EMFs at different intensities, with β-actin used as a loading control. Original blots are presented in Supplementary Fig. 1D. **E** Quantification of *GFAP* protein levels after exposure to ELF-EMFs at different intensities (n = 5). Values are normalized to the 0 mT control group.

a decrease relative to its mRNA level (Fig. 3A, B). Western blot analysis of *NeuN* protein on day 5 also showed reduced expression at 1.0 mT (Fig. 3D, E), suggesting that prolonged exposure to higher ELF-EMF intensities (1.0 mT) may cause cellular damage not evident at earlier time points. These findings indicated that while higher ELF-EMFs intensities promote cell differentiation, they may also compromise neuronal growth due to potential cellular damage.

Neurite initiation is critical for neuronal morphogenesis and early neural circuit formation^{61,} involving nerve fiber projection, synapse formation, and neuronal maturation. Previous studies have reported that ELF-EMF exposure promotes neurite growth in PC12 cells and dorsal root ganglia, with positive correlations to ELF-EMF frequency and intensity^{34,62}. In our study, we found that ELF-EMFs significantly increased the number and length of neurites specifically at 0.5 mT, while the promotional effect was diminished at 1.0 mT (Fig. 4F-H). These findings suggest that neurite outgrowth in spinal NSC-derived neurons is sensitive to ELF-EMF intensity, providing a foundation for potential therapeutic applications of ELF-EMFs in SCI repair. Furthermore, our findings indicate that 0.5 mT represents an optimal condition for inducing neuronal differentiation and neurite outgrowth in spinal cord-derived NSCs.

During the development of the nervous system, the family of bHLH transcription factors, including *NeuroG1*, *NeuroG2*, *NeuroD2* and *NeuroD2*, serve as pivotal regulators of neurogenesis, determining neuronal orientation, differentiation, and neural protrusion in embryonic NSCs^{46,47}. A previous study has shown that exposure to

1,800 MHz radiofrequency electromagnetic fields (EMFs) impairs neurite development in embryonic NSCs by downregulating pro-neuronal genes such as NeuroG1 and $NeuroD1^{63}$. However, our results indicate significant upregulation of NeuroG1 and NeuroD1 expression following exposure to ELF-EMFs (50 Hz), highlighting the distinct role of bHLH transcription factors activated by ELF-EMFs in promoting neuronal differentiation and neurite outgrowth in spinal cord-derived NSCs (Fig. 4A-D).

Previous studies have reported that the effects of ELF-EMFs on NSC proliferation and differentiation may be associated with increased VGCCs expression and activity³⁴. For example, in mesenchymal stem cells (MSCs), static magnetic fields promote proliferation by regulating T-type calcium channels and activating the MAPK signaling pathway⁶⁴. In our study, we found that ELF-EMFs upregulate T-type calcium channel mRNA and protein expression across intensities (Fig. 4F-H), but functional activation of T-type current occurred exclusively at 1 mT (Fig. 4I-K). Given this intensity-restricted functional efficacy, further studies are essential to optimize exposure parameters. We propose that the resulting Ca²⁺ influx mediated by T-type calcium channels subsequently activates the transcription and expression of the pro-neuronal genes, such as *NeuroG1* and *NeuroD1*, promoting neuronal differentiation in NSCs. However, the specific downstream signal pathways driving the activation of pro-neuronal genes warrant further investigation.

Among various calcium channel subtypes, T-type calcium channels are highly expressed during early development and have been shown to modulate NSCs proliferation and neuronal differentiation⁶⁵. T-type calcium channels are low-voltage-activated calcium channels, responsible for regulating extracellular Ca²⁺ influx at resting and hyperpolarizing membrane potentials (below –60 mV)²⁹. This distinct gating property makes them particularly responsive in non-excitable cells. Zablotskii et al. reported that magnetic fields can influence ion diffusion via the Lorentz force, potentially altering the membrane potential, which may prevent high-voltage-activated L-type calcium channels from being active⁶⁶. Consequently, both the unique gating property and upregulated expression levels of T-type calcium channels contribute to the predominant effect of ELF-EMFs. It is plausible that the activation and over-expression of T-type calcium channels could initiate depolarization or Ca²⁺ signaling that promotes the recruitment and activation of other channels like L-type calcium channels or downstream effectors, which, in turn, facilitate NSC differentiation into neurons through Ca²⁺-mediated signal pathways.

Despite the valuable insights, several limitations of our study must be acknowledged. First, the duration of ELF-EMF exposure was relatively short (1 h per day for 3 consecutive days), and the long-term effects remain unknown. Further studies are required to establish optimal exposure parameters, such as frequency, intensity, and duration, to maximize therapeutic benefits while minimizing potential adverse effects. Second, while this study provides in vitro evidence, it remains unclear whether these exposure parameters are suitable or effective for in vivo applications or whether ELF-EMF-stimulated neurons can restore physiological function. Third, while *Sox2* is a well-established master regulator of NSC proliferation and self-renewal, incorporating additional markers, such as *HES1/5* or *Lsh/HELLS*, would strengthen the robustness and generalizability of the transcriptional findings^{67,68}.

In summary, our study demonstrates the potential of ELF-EMFs to specifically activate and promote the proliferation and neuronal differentiation of spinal cord-derived NSCs, presenting valuable insights for SCI repair, regenerative medicine, and neuroscience.

Data availability

All data presented in this manuscript are available from the corresponding author upon reasonable request.

Received: 19 March 2025; Accepted: 4 August 2025

Published online: 11 August 2025

References

- Singh, P., Aggarwal, R., Zevin, B., Grantcharov, T. & Darzi, A. A global Delphi consensus study on defining and measuring quality in surgical training. J Am Coll Surg 219, 346–353 e347 (2014). https://doi.org/10.1016/j.jamcollsurg.2014.03.051
- 2. Alizadeh, A., Dyck, S. M. & Karimi-Abdolrezaee, S. Traumatic spinal cord injury: an overview of pathophysiology, models and acute injury mechanisms. Front. Neurol. 10 https://doi.org/10.3389/fneur.2019.00282 (2019).
- 3. Ross, C. L., Syed, I., Smith, T. L. & Harrison, B. S. The regenerative effects of electromagnetic field on spinal cord injury. *Electromagn. Biol. Med.* 36, 74–87. https://doi.org/10.3109/15368378.2016.1160408 (2017).
- Sánchez, J. A. S. et al. Early management of spinal cord injury: WFNS spine committee recommendations. Neurospine 17, 759–784. https://doi.org/10.14245/ns.2040366.183 (2020).
- 5. Hu, X. et al. Spinal cord injury: molecular mechanisms and therapeutic interventions. Signal. Transduct. Tar. 8 https://doi.org/10.1038/s41392-023-01477-6 (2023).
- Zheng, B. & Tuszynski, M. H. Regulation of axonal regeneration after mammalian spinal cord injury. Nat. Rev. Mol. Cell. Biol. 24, 396–413. https://doi.org/10.1038/s41580-022-00562-y (2023).
- 7. Assinck, P., Duncan, G. J., Hilton, B. J., Plemel, J. R. & Tetzlaff, W. Cell transplantation therapy for spinal cord injury. *Nat. Neurosci.* 20, 637–647. https://doi.org/10.1038/nn.4541 (2017).
- 8. Li, J. C. et al. Recent advances in endogenous neural stem/progenitor cell manipulation for spinal cord injury repair. *Theranostics* 13, 3966–3987. https://doi.org/10.7150/thno.84133 (2023).
- 9. Hosseini, S. M., Borys, B. & Karimi-Abdolrezaee, S. Neural stem cell therapies for spinal cord injury repair: an update on recent preclinical and clinical advances. *Brain* 147, 766–793. https://doi.org/10.1093/brain/awad392 (2024).
- Andreotti, J. P. et al. Neural stem cell niche heterogeneity. Semin Cell. Dev. Biol. 95, 42–53. https://doi.org/10.1016/j.semcdb.2019. 01.005 (2019).
- Novak, D. et al. SOX2 in development and cancer biology. Semin Cancer Biol. 67, 74–82. https://doi.org/10.1016/j.semcancer.2019.08.007 (2020).
- 12. Ross, S. E., Greenberg, M. E. & Stiles, C. D. Basic helix-loop-helix factors in cortical development. *Neuron* **39**, 13–25. https://doi.org/10.1016/S0896-6273(03)00365-9 (2003).

- 13. Hawryluk, G. W. et al. An in vivo characterization of trophic factor production following neural precursor cell or bone marrow stromal cell transplantation for spinal cord injury. Stem Cells Dev. 21, 2222–2238. https://doi.org/10.1089/scd.2011.0596 (2012).
- 14. Kawai, M. et al. Long-term selective stimulation of transplanted neural stem/progenitor cells for spinal cord injury improves locomotor function. Cell. Rep. 37 https://doi.org/10.1016/j.celrep.2021.110019 (2021).
- 15. Sabelstrom, H., Stenudd, M. & Frisen, J. Neural stem cells in the adult spinal cord. *Exp. Neurol.* **260**, 44–49. https://doi.org/10.1016/j.expneurol.2013.01.026 (2014).
- 16. Weiss, S. et al. Multipotent CNS stem cells are present in the adult mammalian spinal cord and ventricular neuroaxis. *J. Neurosci.* **16**, 7599–7609. https://doi.org/10.1523/INEUROSCI.16-23-07599.1996 (1996).
- 17. Moreno-Manzano, V. et al. Activated spinal cord ependymal stem cells rescue neurological function. Stem Cells. 27, 733–743. https://doi.org/10.1002/stem.24 (2009).
- Isakovic, J., Slatkovic, F., Jagecic, D., Petrovic, D. J. & Mitrecic, D. Pulsating extremely Low-Frequency electromagnetic fields influence differentiation of mouse neural stem cells towards Astrocyte-like phenotypes: in vitro pilot study. *Int. J. Mol. Sci.* 25 https://doi.org/10.3390/ijms25074038 (2024).
- 19. Tian, H. et al. System-level biological effects of extremely low-frequency electromagnetic fields: an in vivo experimental review. *Front. Neurosci.* 17, 1247021. https://doi.org/10.3389/fnins.2023.1247021 (2023).
- Lai, H. Neurological effects of static and extremely-low frequency electromagnetic fields. Electromagn. Biol. Med. 41, 201–221. https://doi.org/10.1080/15368378.2022.2064489 (2022).
- 21. Gao, Q. et al. Extremely low frequency electromagnetic fields promote cognitive function and hippocampal neurogenesis of rats with cerebral ischemia. *Neural Regen Res.* **16**, 1252–1257. https://doi.org/10.4103/1673-5374.301020 (2021).
- Adel Zalata, A. Z. E. S. & Shaalan, D. Youssef El-Baiomy, taymour mostafa. In vitro effect of cell phone radiation on motility, DNA fragmentation and clusterin gene expression in human sperm. *Int. J. Fertil. Steril.* 9, 129–136. https://doi.org/10.22074/ijfs.2015.4 217 (2015).
- Linnemann, C. et al. NET formation was reduced via exposure to extremely Low-Frequency pulsed electromagnetic fields. Int. J. Mol. Sci. 24 https://doi.org/10.3390/ijms241914629 (2023).
- 24. Pesce, M., Patruno, A., Speranza, L. & Reale, M. Extremely low frequency electromagnetic field and wound healing: implication of cytokines as biological mediators. *Eur. Cytokine Netw.* 24, 1–10. https://doi.org/10.1684/ecn.2013.0332 (2013).
- Zheng, Y., Cheng, J. H., Dong, L., Ma, X. X. & Kong, Q. Y. Effects of exposure to extremely low frequency electromagnetic fields on hippocampal long-term potentiation in hippocampal CA1 region. *Biochem. Bioph Res. Co.* 517, 513–519. https://doi.org/10.1016/ j.bbrc.2019.07.085 (2019).
- 26. Zheng, Y., Xia, P., Dong, L., Tian, L. & Xiong, C. Effects of modulation on sodium and potassium channel currents by extremely low frequency electromagnetic fields stimulation on hippocampal CA1 pyramidal cells. *Electromagn. Biol. Med.* 40, 274–285. https://doi.org/10.1080/15368378.2021.1885433 (2021).
- Xia, P., Zheng, Y., Dong, L. & Tian, C. X. Short-Term extremely Low-Frequency electromagnetic field inhibits synaptic plasticity of Schaffer Collateral-CA1 synapses in rat hippocampus via the ca/calcineurin pathway. Acs Chem. Neurosci. 12, 3550–3557. https://doi.org/10.1021/acschemneuro.1c00500 (2021).
- 28. Cecchetto, C., Maschietto, M., Boccaccio, P. & Vassanelli, S. Electromagnetic field affects the voltage-dependent potassium channel Kv1.3. *Electromagn. Biol. Med.* 39, 316–322. https://doi.org/10.1080/15368378.2020.1799386 (2020).
- 29. Berridge, M. J. & Lipp, M. D. B. P. Calcium a life and death signal. Nature 395, 645-648. https://doi.org/10.1038/27094 (1998).
- 30. du Sert, N. P. et al. Reporting animal research: explanation and elaboration for the ARRIVE guidelines 2.0. *Plos Biol.* **18** https://doi.org/10.1371/journal.pbio.3000411 (2020).
- 31. Hugnot, J. P. Isolate and culture neural stem cells from the mouse adult spinal cord. *Methods Mol. Biol.* **2389**, 45–56. https://doi.org/10.1007/978-1-0716-1783-0_4 (2022).
- 32. He, Y. L. et al. Exposure to extremely low-frequency electromagnetic fields modulates Na+currents in rat cerebellar granule cells through increase of AA/PGE2 and EP receptor-mediated cAMP/PKA pathway. *PLoS One.* **8**, e54376. https://doi.org/10.1371/jour nal.pone.0054376 (2013).
- 33. Leone, L., Podda, M. V. & Grassi, C. Impact of electromagnetic fields on stem cells: common mechanisms at the crossroad between adult neurogenesis and osteogenesis. *Front. Cell. Neurosci.* 9, 228. https://doi.org/10.3389/fncel.2015.00228 (2015).
- 34. Piacentini, R., Ripoli, C., Mezzogori, D., Azzena, G. B. & Grassi, C. Extremely low-frequency electromagnetic fields promote in vitro neurogenesis via upregulation of Ca(v)1-channel activity. *J. Cell. Physiol.* 215, 129–139. https://doi.org/10.1002/jcp.21293 (2008)
- 35. Chen, C. et al. Excess thyroid hormone inhibits embryonic neural stem/progenitor cells proliferation and maintenance through STAT3 signalling pathway. *Neurotox. Res.* 20, 15–25. https://doi.org/10.1007/s12640-010-9214-y (2011).
- Ma, Q. et al. Extremely Low-Frequency electromagnetic fields promote in vitro neuronal differentiation and neurite outgrowth of embryonic neural stem cells via Up-Regulating TRPC1. PLoS One. 11, e0150923. https://doi.org/10.1371/journal.pone.0150923 (2016).
- 37. Deleyrolle, L. P. & Reynolds, B. A. Isolation, expansion, and differentiation of adult mammalian neural stem and progenitor cells using the neurosphere assay. *Methods Mol. Biol.* **549**, 91–101. https://doi.org/10.1007/978-1-60327-931-4_7 (2009).
- 38. Meijering, E. et al. Design and validation of a tool for neurite tracing and analysis in fluorescence microscopy images. *Cytom Part.* A. 58a, 167–176. https://doi.org/10.1002/cyto.a.20022 (2004).
- 39. Fan, W. Y. et al. L-Type calcium channel modulates Low-Intensity pulsed Ultrasound-Induced excitation in cultured hippocampal neurons. *Neurosci. Bull.* 40, 921–936. https://doi.org/10.1007/s12264-024-01186-2 (2024).
- 40. Dreyfus, F. M. et al. Selective T-type calcium channel block in thalamic neurons reveals channel redundancy and physiological impact of I(T)window. J. Neurosci. 30, 99–109. https://doi.org/10.1523/JNEUROSCI.4305-09.2010 (2010).
- 41. Wang, T. et al. Research progress on the mechanisms of endogenous neural stem cell differentiation in spinal cord injury repair. Front. Cell. Neurosci. 19 https://doi.org/10.3389/fncel.2025.1592297 (2025).
- 42. Bernhardt, R. & Matus, A. Light and electron microscopic studies of the distribution of microtubule-associated protein 2 in rat brain: a difference between dendritic and axonal cytoskeletons. *J. Comp. Neurol.* 226, 203–221. https://doi.org/10.1002/cne.90226 0205 (1984).
- 43. Petrovic, D. J., Jagecic, D., Krasic, J., Sincic, N. & Mitrecic, D. Effect of fetal bovine serum or basic fibroblast growth factor on cell survival and the proliferation of neural stem cells: the influence of homocysteine treatment. *Int. J. Mol. Sci.* 24 https://doi.org/10.3 390/ijms241814161 (2023).
- 44. Plecas, A., Kapuralin, K., Grandverger, L., Mitrecic, D. & Alic, I. Thy1-YFP: an effective tool for single cell tracing from neuronal progenitors to mature functionally active neurons. Cell. Death Discov. 11, 18. https://doi.org/10.1038/s41420-025-02297-z (2025).
- 45. Graham, V., Khudyakov, J., Ellis, P. & Pevny, L. SOX2 functions to maintain neural progenitor identity. *Neuron* **39**, 749–765. https://doi.org/10.1016/s0896-6273(03)00497-5 (2003).
- 46. Soldatov, R. et al. Spatiotemporal structure of cell fate decisions in murine neural crest. *Science* **364**, 971–. https://doi.org/10.1126/science.aas9536 (2019).
- 47. Murre, C. Helix-loop-helix proteins and the advent of cellular diversity: 30 years of discovery. *Gene Dev.* 33, 6–25. https://doi.org/10.1101/gad.320663.118 (2019).
- 48. Cuccurazzu, B. et al. Exposure to extremely low-frequency (50 Hz) electromagnetic fields enhances adult hippocampal neurogenesis in C57BL/6 mice. Exp. Neurol. 226, 173–182. https://doi.org/10.1016/j.expneurol.2010.08.022 (2010).

- 49. Louhivuori, L. M. et al. Role of low voltage activated calcium channels in neuritogenesis and active migration of embryonic neural progenitor cells. Stem Cells Dev. 22, 1206–1219. https://doi.org/10.1089/scd.2012.0234 (2013).
- 50. Britz, O. et al. A role for proneural genes in the maturation of cortical progenitor cells. Cereb. Cortex. 16 https://doi.org/10.1093/cercor/bhj168 (2006).
- Perez-Reyes, E. Molecular physiology of low-voltage-activated t-type calcium channels. *Physiol. Rev.* 83, 117–161. https://doi.org/10.1152/physrev.00018.2002 (2003).
- 52. Allen, N. J. & Lyons, D. A. Glia as architects of central nervous system formation and function. Science 362, 181-. https://doi.org/10.1126/science.aat0473 (2018).
- 53. Meletis, K. et al. Spinal cord injury reveals multilineage differentiation of ependymal cells. *Plos Biol.* **6**, 1494–1507. https://doi.org/10.1371/journal.pbio.0060182 (2008).
- 54. Santini, M. T., Rainaldi, G. & Indovina, P. L. Cellular effects of extremely low frequency (ELF) electromagnetic fields. *Int. J. Radiat. Biol.* 85, 294–313. https://doi.org/10.1080/09553000902781097 (2009).
- 55. Sun, J. et al. Effects of extremely low frequency electromagnetic fields on the tumor cell Inhibition and the possible mechanism. *Sci. Rep-Uk.* 13 https://doi.org/10.1038/s41598-023-34144-5 (2023).
- Kobayashi-Sun, J. et al. Extremely low-frequency electromagnetic fields facilitate both osteoblast and osteoclast activity through Wnt/beta-catenin signaling in the zebrafish scale. Front. Cell. Dev. Biol. 12, 1340089. https://doi.org/10.3389/fcell.2024.1340089 (2024).
- 57. Moya-Gomez, A. et al. Extremely Low-Frequency electromagnetic stimulation (ELF-EMS) improves neurological outcome and reduces microglial reactivity in a rodent model of global transient stroke. *Int. J. Mol. Sci.* 24 https://doi.org/10.3390/ijms241311117 (2023)
- 58. Grassi, C. et al. Effects of 50 hz electromagnetic fields on voltage-gated Ca channels and their role in modulation of neuroendocrine cell proliferation and death. *Cell. Calcium.* 35, 307–315. https://doi.org/10.1016/j.ceca.2003.09.001 (2004).
- 59. Sherafat, M. A. et al. Electromagnetic field stimulation potentiates endogenous Myelin repair by recruiting subventricular neural stem cells in an experimental model of white matter demyelination. *J. Mol. Neurosci.* 48, 144–153. https://doi.org/10.1007/s1203 1-012-9791-8 (2012).
- 60. de Castro, F. et al. Extremely Low-Frequency electromagnetic fields affect transcript levels of neuronal Differentiation-Related genes in embryonic neural stem cells. *PLoS ONE*. 9 https://doi.org/10.1371/journal.pone.0090041 (2014).
- 61. Zhang, S. X., Duan, L. H., He, S. J., Zhuang, G. F. & Yu, X. Phosphatidylinositol 3,4-bisphosphate regulates neurite initiation and dendrite morphogenesis via actin aggregation. Cell. Res. 27, 253–273. https://doi.org/10.1038/cr.2017.13 (2017).
- 62. Zhang, Y., Ding, J. & Duan, W. A study of the effects of flux density and frequency of pulsed electromagnetic field on neurite outgrowth in PC12 cells. J. Biol. Phys. 32, 1–9. https://doi.org/10.1007/s10867-006-6901-2 (2006).
- Chen, C. et al. Exposure to 1800 mhz radiofrequency radiation impairs neurite outgrowth of embryonic neural stem cells. Sci. Rep. 4, 5103. https://doi.org/10.1038/srep05103 (2014).
- 64. Wu, H. K. F. et al. Static magnetic fields regulate T-Type calcium ion channels and mediate mesenchymal stem cells proliferation. Cells-Basel 11 https://doi.org/10.3390/cells11152460 (2022).
- 65. Rebellato, P. et al. The T-type Ca channel Ca3.2 regulates differentiation of neural progenitor cells during cortical development via Caspase-3. *Neuroscience* 402, 78–89. https://doi.org/10.1016/j.neuroscience.2019.01.015 (2019).
- Zablotskii, V., Polyakova, T. & Dejneka, A. Cells in the Non-Uniform magnetic world: how cells respond to High-Gradient magnetic fields. *Bioessays* 40 https://doi.org/10.1002/bies.201800017 (2018).
- 67. Han, Y. et al. Lsh/HELLS regulates self-renewal/proliferation of neural stem/progenitor cells. Sci. Rep. 7, 1136. https://doi.org/10.1 038/s41598-017-00804-6 (2017).
- 68. Ahmed, S. et al. Transcription factors and neural stem cell self-renewal, growth and differentiation. *Cell. Adh Migr.* 3, 412–424. https://doi.org/10.4161/cam.3.4.8803 (2009).

Acknowledgements

This work was supported by the Science and Technology Innovation 2030 - Brain Science and Brain-Inspired Intelligence Project (2021ZD0201301), the National Key Research & Development Program of China (2022YFC3602700, 2022YFC3602702), the National Natural Science Foundation of China (32170688), the Shanghai Municipal Science and Technology Major Project (2018SHZDZX01), the Shanghai Songjiang District Science and Technology Research Project (22SJKJGG5).

Author contributions

L.X. and W.X. designed the research; W.X.T. performed most of the experiments and drafted the manuscript; D.H., X.F.L., Y.F., Y.X., and J.W.H. helped with the experiments; L.X. reviewed the manuscript and supervised the project.

Declarations

Competing interests

The authors declare no competing interests.

Additional information

Supplementary Information The online version contains supplementary material available at https://doi.org/10.1038/s41598-025-14738-x.

Correspondence and requests for materials should be addressed to W.X. or L.X.

Reprints and permissions information is available at www.nature.com/reprints.

Publisher's note Springer Nature remains neutral with regard to jurisdictional claims in published maps and institutional affiliations.

Open Access This article is licensed under a Creative Commons Attribution-NonCommercial-NoDerivatives 4.0 International License, which permits any non-commercial use, sharing, distribution and reproduction in any medium or format, as long as you give appropriate credit to the original author(s) and the source, provide a link to the Creative Commons licence, and indicate if you modified the licensed material. You do not have permission under this licence to share adapted material derived from this article or parts of it. The images or other third party material in this article are included in the article's Creative Commons licence, unless indicated otherwise in a credit line to the material. If material is not included in the article's Creative Commons licence and your intended use is not permitted by statutory regulation or exceeds the permitted use, you will need to obtain permission directly from the copyright holder. To view a copy of this licence, visit http://creativecommons.org/licenses/by-nc-nd/4.0/.

© The Author(s) 2025